

# Combining Pharmacophore Fingerprints and PLS-Discriminant Analysis for Virtual Screening and SAR Elucidation

Sune Askjaer<sup>\*,†,‡</sup> and Morten Langgård<sup>‡</sup>

Department of Medicinal Chemistry, Faculty of Pharmaceutical Sciences, University of Copenhagen, DK-2100 Copenhagen, Denmark, and Department of Computational Chemistry, H. Lundbeck A/S, Ottiliavej 9, DK-2500 Copenhagen, Valby, Denmark

Received September 26, 2007

The criterion of success for the initial stages of a ligand-based drug-discovery project is dual. First, a set of suitable lead compounds has to be identified. Second, a level of a preliminary structure–activity relationship (SAR) of the identified ligands has to be established in order to guide the lead optimization toward a final drug candidate. This paper presents a combined approach to solving these two problems of ligand-based virtual screening and elucidation of SAR based on interplay between pharmacophore fingerprints and interpretation of PLS-discriminant analysis (PLS-DA) models. The virtual screening capability of the PLS-DA method is compared to group fusion maximum similarity searching in a test using four graph-based pharmacophore fingerprints over a range of 10 diverse targets. The PLS-DA method was generally found to do better than the  $S_{\max}$  method. The GpiDAPH3 and PCH fingerprints proved superior to the TGT and TGD fingerprints. Examples of SAR elucidation based on PLS-DA model interpretation of model coefficients using a reversible pharmacophore fingerprint are given. In addition, we tested the hypothesis that feature combinations coming from the analysis of two-dimensional (2D) pharmacophore fingerprints could be used to elucidate a three-dimensional pharmacophore (Williams, C. *Mol. Diversity* **2006**, *10* (3), 311–332). This test was performed by mapping of pharmacophore triplets found by the PLS-DA model to be important for activity onto relevant ligands aligned by the protein-binding site known from X-ray complexes. The result of this analysis assists in explaining the efficiency of 2D pharmacophore fingerprints as descriptors in virtual screening.

## 1. INTRODUCTION

The mining of data for patterns relating to the ligand–target recognition process has become an essential part of the early stages of the drug-discovery process.<sup>1–3</sup> It is not uncommon that drug-discovery projects are able to start with information about at least a handful of diverse active compounds. This situation is due to the accumulated information available in public and proprietary databases,<sup>4,5</sup> journals, and patents complemented by results from high throughput screening (HTS).<sup>6</sup> In cases where no three-dimensional (3D) structural information on the target is available, this initial set of ligands has to form the basis for the early stages of the discovery process. The criterion of success for this process is dual.<sup>7</sup> First of all, it is essential to identify new hit compounds that lie beyond the previously explored chemistry space of the known ligands. This task is usually engaged with virtual screening methods from the chemoinformatics toolbox, including similarity searching<sup>8,9</sup> and machine learning techniques.<sup>10,11</sup> Second, it is important to reach a preliminary understanding of the basic structure–activity relationship (SAR) exhibited by the various ligands.<sup>12</sup> This understanding is vital to the generation of a pharmacophore hypothesis describing the pharmacophoric pattern

that relates to the recognition of the ligand at the binding site. Such a hypothesis is an important tool in lead optimization and for aligning ligands for 3D pharmacophore model generation, etc. The usual tools for generating the initial pharmacophore hypotheses are based on force fields and stochastic or brute-force-driven 3D alignment approaches implemented in programs like GASP,<sup>13</sup> Catalyst,<sup>14</sup> and MOE<sup>15</sup> or, in other ways, are dependent on 3D prealignments of reference ligands like the SQUID<sup>16</sup> approach. However, these approaches are computationally demanding, and it can be very difficult to rank the multiple solutions that they generate correctly.

In this paper, we describe a combined approach to solving the dual tasks of finding hit compounds and deriving SAR information. By using a reversible pharmacophore fingerprint in combination with a PLS-based discriminative analysis procedure (PLS-DA), we have developed a procedure that combines virtual screening and SAR elucidation via direct model interpretation. In order to validate the procedure, we have set up a retrospective virtual screening scenario to investigate the virtual screening performance of the PLS-DA method. This includes a benchmark of the reversible pharmacophore fingerprint against other types of pharmacophore fingerprints. Finally, we investigate how PLS-DA models based on training sets containing a small number of actives can be used to derive important SAR information at the pharmacophoric level. The PLS-DA method generates a linear model that allows for direct model interpretation by

\* Corresponding author phone: +45 3643-2926; fax: +45 3643-8237; e-mail: suap@lundbeck.com.

<sup>†</sup> Department of Medicinal Chemistry, Faculty of Pharmaceutical Sciences.

<sup>‡</sup> Department of Computational Chemistry.

**Table 1.** Biological Target and the Mean Pairwise Similarity within Each Activity Class of the 250 Selected Compounds Measured with the Four Different Fingerprints and the Tanimoto Coefficient

inhibitor target	target abbreviation	mean pairwise Tanimoto similarity within 250 compounds in target class by fingerprint			
		GpiDAPH3	PCH	TGT	TGD
Serotonin transporter	5-HTT	0.019	0.058	0.324	0.430
Adenosine A1 receptor	A1A	0.062	0.073	0.328	0.488
cyclooxygenase-2	COX-2	0.057	0.080	0.359	0.513
Dopamine D2 receptor	D2	0.016	0.052	0.331	0.459
HIV type 1 retropepsin	HIV-1 P	0.061	0.097	0.422	0.533
Tachykinin NK1 receptor	NK1	0.036	0.089	0.342	0.466
Ionotropic Glutamate type 2 receptor	NMDA	0.019	0.034	0.263	0.382
cAMP phosphodiesterase 4	PDE 4	0.055	0.085	0.378	0.523
Opioid receptor delta-type	Opioid D	0.044	0.097	0.356	0.475
Thrombin-activated blood factor II	Thrombin	0.032	0.087	0.436	0.520
average overall targets		0.040	0.075	0.354	0.479

inspection of model coefficients. This transparency of the PLS-DA model is an advantage over other machine learning techniques that operate in nonlinear dimensions where model interpretation is difficult. We have utilized this advantage to derive pharmacophore-based SAR information using a reversible two-dimensional (2D), three-point pharmacophore fingerprint that encodes the pharmacophore feature types in the same way as the regular 3D pharmacophore annotation scheme in the MOE software.<sup>15</sup> As a benchmarking reference in the virtual screening, we have chosen to include the group fusion maximum similarity searching method ( $S_{\max}$ ; Hert, J.; Willett, P.; Wilton, D. J. *J. Chem. Inf. Comput. Sci.* **2004**, *44* (3), 1177–1185) in this study. This method has been extensively used and performs well with both small and larger numbers of active compounds.<sup>2</sup>

The study is comprised of two parts. The first part treats the results of the retrospective virtual screening experiment of PLS-DA and  $S_{\max}$  using four different kinds of pharmacophore fingerprints. The PLS-DA and  $S_{\max}$  methods are compared in terms of both their overall performance and early recognition of active ligands. In addition, the four different fingerprints are benchmarked and compared. In the second part, we look in detail at the PLS-DA models and at the possibilities for elucidating SAR information from these models.

## 2. METHODS

**2.1. Pharmacophore Fingerprints as Descriptors.** The four different pharmacophore fingerprints treated in this study are all graph-based and part of the MOE software. They are as follows: Typed Graph Distance (TGD), Typed Graph Triangle (TGT), Graph  $\pi$ -Donor–Acceptor–Polar–Hydrophobe triangle (GpiDAPH3), and 2D Polar-Charged-Hydrophobe triangles (PCH).<sup>2,15</sup> We have modified the standard PCH fingerprint to exclude metal ligand pharmacophore features because these feature types are not included in the other fingerprint types either. The fingerprints differ in complexity, with the simplest being the TGD, which only encodes pharmacophore feature pairs, whereas the other types encode pharmacophore feature triplets. The GpiDAPH3, TGT, and TGD assign pharmacophore feature properties to all atoms, whereas the PCH scheme uses centroids for features originating from multiple atoms. The complexity and length of the triplet fingerprints increase from the TGT over the PCH to the GpiDAPH3 fingerprint that also

discriminates between features with and without  $\pi$  electrons. The PCH fingerprint supports back-translation or reversal from the hashed fingerprint bit codes back to the origination pharmacophore feature triplets of a compound via an SVL (the programming language used within MOE) application developed and described by Williams.<sup>2</sup> This functionality allows for feature triplet visualization by projection of the triplet onto any compound that contains the selected triplet. We have adapted this application by Williams to handle PLS-DA models and used it for visualization of important pharmacophore features by projection of fingerprint feature triplets identified by the PLS-DA models onto sets of ligands.

**2.2. The Dataset.** The dataset for this study was generated with the aim of maximizing the compound diversity for each target. The dataset was derived from two sources. A compilation of active compounds were selected from the Wombat database,<sup>5</sup> while a larger number of decoy compounds were retrieved from an in-house database of commercially available lead-like compounds. The active compounds represent inhibitors from 10 different targets spanning enzymes, receptors, ion channels, and neurotransmitters. The targets were selected among those in Wombat that contained the highest number of compounds in an effort to include as diverse a set of chemical structures for each target as possible. The active compounds for each target were filtered to include only compounds with affinity stronger than 1  $\mu$ M (reported as either  $IC_{50}$  or  $K_i$ ) for that given activity class and 40 or fewer heavy atoms. From the remaining compounds, sets of 250 diverse compounds from each activity class were selected with the standard diverse subset algorithm in MOE using the GpiDAPH3 fingerprint and the Tanimoto similarity measure. This filtering step removed between 65% and 91% of the compounds within each activity class and was performed to reduce the number of near analogues in the dataset. However, with as many as 250 compounds remaining in each activity class, there are still going to be some compounds that are relatively closely structurally related. The composition and diversity of the active set measured as the mean pairwise similarity can be seen in Table 1. From the mean pairwise similarities, it is clear that the diversity within the different classes differs to some extent. The diversity is naturally influenced by the promiscuity of the target and the varying medicinal chemistry efforts around it.

To serve as decoys, 10 000 lead-like compounds with 40 or fewer heavy atoms were randomly selected from an in-house database containing more than one million com-

mercially available compounds. The decoy compounds were selected to give the dataset a composition similar to that of a medium-sized screening set. The affinities of the decoys for any of the 10 selected targets are unknown but presumed to be zero. From the joint dataset containing  $10 \times 250$  active and 10 000 decoy compounds, a training set consisting of 10% from each activity class was selected at random while the remaining 90% were used as an external test set. Thus, for each activity class, the PLS-DA training set contains 25 known actives and 1225 putative inactives, while the test set holds 225 known actives and 11 025 putative inactives. During model building and subsequent evaluation for each given activity class, the remaining nine other classes and the decoy set were all considered inactive, ignoring possible cross-activity between the targets. By randomly selecting 25 actives for the training set from each target, not all test set compounds are going to be equally well represented by the actives in the training set. Some test set compounds will be relatively near analogues to the training set compounds, but the majority will only be remotely related. This situation produces a more realistic virtual screening scenario, where the training set composition is not equally representative of the active compounds in the collection screened.

### 2.3. PLS-DA for Ranking and Model Interpretation.

The PLS-DA method used for ranking and model interpretation is similar to the PLS method used in QSAR analysis, with the only difference being that the response variable is binary (1 for active compounds and 0 for inactive compounds) instead of continuous. The method has previously been applied for classification using 2D chemical descriptors,<sup>17</sup> atom pair descriptors,<sup>18</sup> BCUT descriptors,<sup>19</sup> and a combination of 2D physicochemical descriptors, fragments, and short two-point pharmacophore fingerprints.<sup>20</sup> The PLS-DA method is an extension of the trend vector (TV) method,<sup>21</sup> which only uses the first moment or principle component (PC) extracted from the descriptor matrix. PLS-DA and TV analyses have in the past been used for substructural analysis<sup>20,22</sup> to identify atom pair descriptors, fragments, and two-point 2D pharmacophores relating to activity. The TV method has recently been benchmarked for virtual screening using atom pair descriptors against a wide range of other machine learning classification methods like support vector machines (SVMs), naïve Bayesian (NB) classifiers, artificial neural networks (ANNs), random forest (RF), decision trees (DSs),<sup>11</sup> and binary kernel discrimination (BKD),<sup>23</sup> where it was shown to give very high initial enrichment, outperforming other methods on the first fraction of the dataset. The properties of the PLS-DA method for overall performance and early recognition have received little attention.

In the current study, we are applying the PLS-DA method for virtual screening and SAR elucidation based on small-to medium-sized training sets containing 25 active compounds from each class. This relatively small number is selected to simulate a drug-discovery project based on an HTS campaign and/or information from the literature. Our descriptor basis for the virtual screening experiment is the four different 2D pharmacophore fingerprints ranging from short two-point to longer and more complex three-point pharmacophore feature triplets. To illustrate how SAR information can be derived from such models, we interpret a subset of the models built using the reversible PCH

fingerprint to identify feature triplets relating to activity and show how these can be used to generate pharmacophore hypotheses.

**2.4. PLS-DA Modeling Procedure.** The pharmacophore fingerprints of the training set compounds were calculated in MOE and exported as a bit matrix to the SIMCA-P program<sup>24</sup> where the PLS-DA models were built. All fingerprint bits that only occurred once or twice in the total training set were disregarded because these contain very little information across the training set as a whole and make the size of the bit matrix swell significantly. In addition, fingerprint bits that were found in more than half of the compounds of the full training set were discarded because they were presumed to be too general to relate to the recognition between the ligand and the binding site. From the remaining fingerprint bits, a union bit string of length  $n$  was created for each of the  $m$  training set compounds so that a bit matrix of size  $n \times m$  was obtained. This bit matrix was imported into SIMCA-P, where a two-class PLS-DA was performed on the unscaled and uncentered bit matrix.

The binary PLS regression procedure extracts succeeding PCs from the training data describing that variance of the fingerprint data that best discriminates active compounds from inactive ones. New PCs are added to the model as long as  $q^2$ , a measure of the overall predicted membership scores of a 7-fold cross-validation jack-knifing procedure, improves.<sup>25,26</sup> When no further improvement in  $q^2$  is observed, the addition of PCs stops to prevent overfitting, and the model is saved as the cumulative PC coefficient vector. The  $q^2$  statistics from a 7-fold cross-validation are known to be a good measure of model predictability<sup>26,27</sup> for both QSAR and 3D QSAR models where the dependent variable is continuous. The class membership prediction  $Y$ , for a compound  $j$ , is obtained as the dot product of the model coefficient vector  $\mathbf{a}$  and the fingerprint bit string of the compound  $x_j$ .

$$Y(x_j) = \sum_{i=1}^n a_i \cdot x_{ij} + b_0$$

**2.5. Model Interpretation and SAR Elucidation.** The linear nature of the PLS-DA model allows for easy and direct interpretation of the model via the sign and magnitude of the coefficients of  $\mathbf{a}$ . High positive and negative coefficients correspond to fingerprint bits that relate to higher or lower class membership scores, respectively. This straightforward relationship is a clear advantage over most other machine learning methods, such as SVM, ANN, RF, DF, and BKD, where model interpretation, e.g., via substructural analysis,<sup>22</sup> is difficult. Of the popular machine learning methods, only NB classifiers<sup>28</sup> offer possibilities for easy model interpretation comparable to that of linear models. Franke et al.<sup>29</sup> have devised a computationally intensive technique for extraction and visualization of important isolated pharmacophore features from an SVM model. However, we feel that looking at pharmacophore feature triplets provides more information than the isolated features because the triplets provide a better basis for creating alignments of the important features in two dimensions. Such relative alignments can be used to create 2D pharmacophore hypotheses that can possibly be extended into three dimensions via the use of force fields and interligand feature–feature constraints.



**2.6. Group Fusion  $S_{\max}$  Method.** Recently, the group fusion similarity searching method using multiple reference structures has received much attention.<sup>2,30,31</sup> Because this method is widely used and performs well using small sets of diverse query compounds, we have chosen it for comparison with PLS-DA. The group fusion similarity score can be calculated as either the sum, average, or maximum similarity between a compound and the query structures. Several studies<sup>1,2,9</sup> have found the Tanimoto measure and the maximum similarity fusion rule to be the most efficient combination for multireference structure similarity searching. The group fusion maximum similarity ( $S_{\max}$ ) of compound  $j$  is calculated as the maximum Tanimoto similarity between  $j$  and any one of the query compounds  $i$  belonging to a set of known actives.

$$S_{\max}(j) = \max\{S(1,j), S(2,j), \dots, S(i,j)\}$$

The group fusion maximum similarity scores were calculated with the MOE software<sup>15</sup> and ranked according to the  $S_{\max}$  score. For each target, the same 25 actives that were used for the PLS-DA training were also used for the group fusion query set. Because the group fusion similarity measure treats all parts of a compound equally, it cannot be interpreted on a substructural level.

**2.7. Measuring the Discriminative Power.** The test set compounds are sorted according to the class membership score for PLS-DA models and  $S_{\max}$  for the group fusion. The resulting rank is used to measure the performance of the classification of the different fingerprints in combination with the two methods. The area under the curve (AUC) of the receiver operator characteristic<sup>32,33</sup> (ROC) is used as a metric to assess the overall sensitivity and specificity exchange of the various fingerprints and method combinations. The sensitivity or recall corresponds to the true positive rate, while  $1 - \text{specificity}$  corresponds to the rate of false positives. Models with perfect prediction, ranking all actives higher than any of the inactives, will produce an ROC AUC of 1, whereas a perfectly random model will produce a ROC curve with AUC = 0.5. However, as was recently pointed out by Truchon and Bayly,<sup>34</sup> the AUC of the ROC curve is not a fully valid lone-standing measure to use for benchmarking methods for virtual screening. This is because virtual screening usually involves very large databases and the in vitro screening resources usually only allow for experimental screening of the absolutely top-ranking fraction of large databases. However, the ROC AUC gives an indication of how good the models are to capture both early and broad recognition of the patterns of compounds belonging to a given target class. If the broad recognition of the actives is missing, the latter part of the actives will be picked up more or less by random, well mixed in with the inactives, resulting in a lower ROC AUC. The measure therefore gives a suggestion of the properties of the methods for the overall recognition of actives. In terms of high-throughput virtual screening, this measure is not as important as the early recognition of actives, but it is still relevant because it tells us about the models' abilities at finding hits that are further from the training set compounds and thus possibly outside of the known chemistry space of the target. To assess the early recognition of the actives directly, we looked at the fraction of actives found in the top ranking 1% of the test

**Table 2.** Spearman Rank ( $\rho$ ) of the Intraclass Mean Pairwise Similarity (Table 1) of the Different Fingerprints over the 10 Classes<sup>a</sup>

Spearman rank $\rho$	GpiDAPH3	PCH	TGT	TGD
GpiDAPH3	1	0.48	0.39	0.71
PCH	0.48	1	0.71	0.62
TGT	0.39	0.71	1	0.89
TGD	0.71	0.62	0.89	1

<sup>a</sup> The  $\rho$  values describe the rank-order correlation between pairs of class similarity ranks. A  $\rho$  value of 1 indicates a perfect rank-order correlation, and  $\rho = 0$  corresponds to no correlation.

set. Because the number of actives and inactives are the same for all targets, the retrieval at 1% can be compared directly across all targets. The ROC AUC should primarily be used to judge the overall performance of the methods, supplemented by recall at 1% and visual inspection of the ROC curves to assess which method gives the best early recognition of actives. Hence, given two different methods that give rise to ROC curves with similar AUCs, the one causing the steepest initial ascent should thus be preferred over the other.

### 3. RESULTS AND DISCUSSION

**3.1. The Dataset.** The mean pairwise intraclass similarity listed in Table 1 shows that the different complexities and lengths of the pharmacophore fingerprints give very different perceptions of diversity within each class. The class-averaged mean pairwise similarity spans from 0.48 for the TGD to as low as 0.04 for the GpiDAPH3 fingerprint, illustrating that the latter fingerprint is much longer and more sparsely populated than the former. The relative rank order of intraclass diversity differs between the different fingerprints, as is demonstrated by the Spearman ranks shown in Table 2.

Measured by the rank of mean pairwise similarity, the TGT and TGD fingerprints are the most strongly correlated, while the GpiDAPH3–TGT and GpiDAPH3–PCH fingerprint pairs are the most dissimilar pairs.

**3.2. Comparison of Ranking Methods and Fingerprints.** For both PLS-DA and  $S_{\max}$ , all four pharmacophore fingerprints were used separately to construct models for each of the 10 targets using the training set. The resulting 80 models were used to rank the test set and measure the discriminative power of the individual target–fingerprint–method combinations. The overall discriminative performances of these combinations measured as the AUC of the test set ROC curves are summarized in Figure 1.

**Comparison of PLS-DA and  $S_{\max}$ .** In 39 of the 40 cases (with the exception being GpiDAPH3 on PDE4), the PLS-DA models outperform the group fusion  $S_{\max}$  method measured as ROC AUC. The overall performance difference between the two methods is largest and most consistent for the shorter and simpler TGT and TGD fingerprints. With these two fingerprint types, all of the PLS-DA models show markedly better performance than the group fusion method. In general, the PLS-DA GpiDAPH3 and PCH models do best, but one of the two fingerprints cannot be preferred over the other because their relative performance varies across the different targets. For the GpiDAPH3 and PCH fingerprints, the relative performance differences between the PLS-DA and  $S_{\max}$  methods appear smaller than those for the TGT and TGD fingerprints. This smaller difference should,

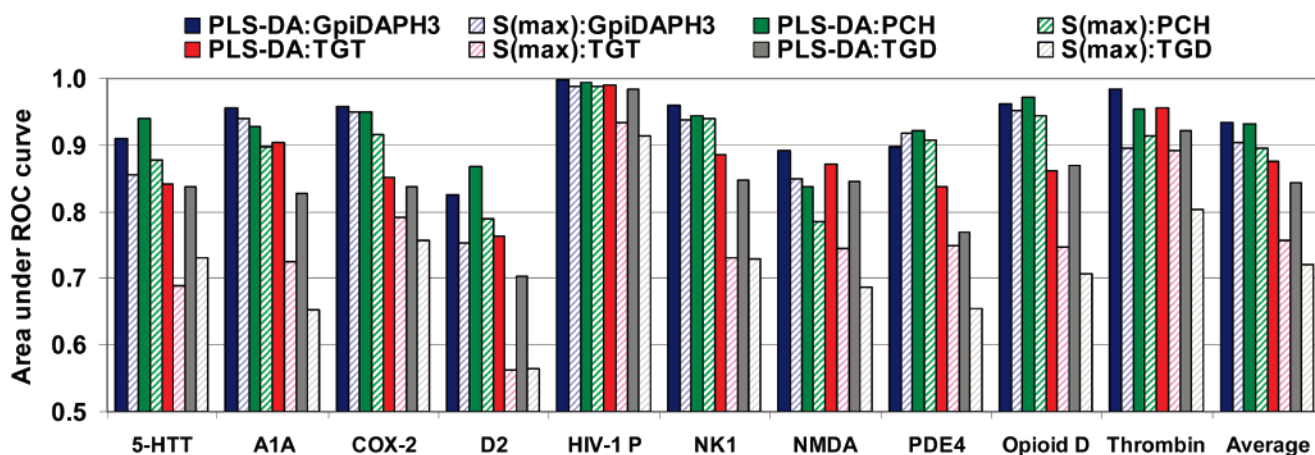


**Figure 1.** Area under the ROC curve for test set ranking using PLS-DA (solid bars) and group fusion  $S_{\max}$  (dashed bars) with the four different fingerprints; GpiDAPH3, PCH, TGT, and TGD for all 10 targets.

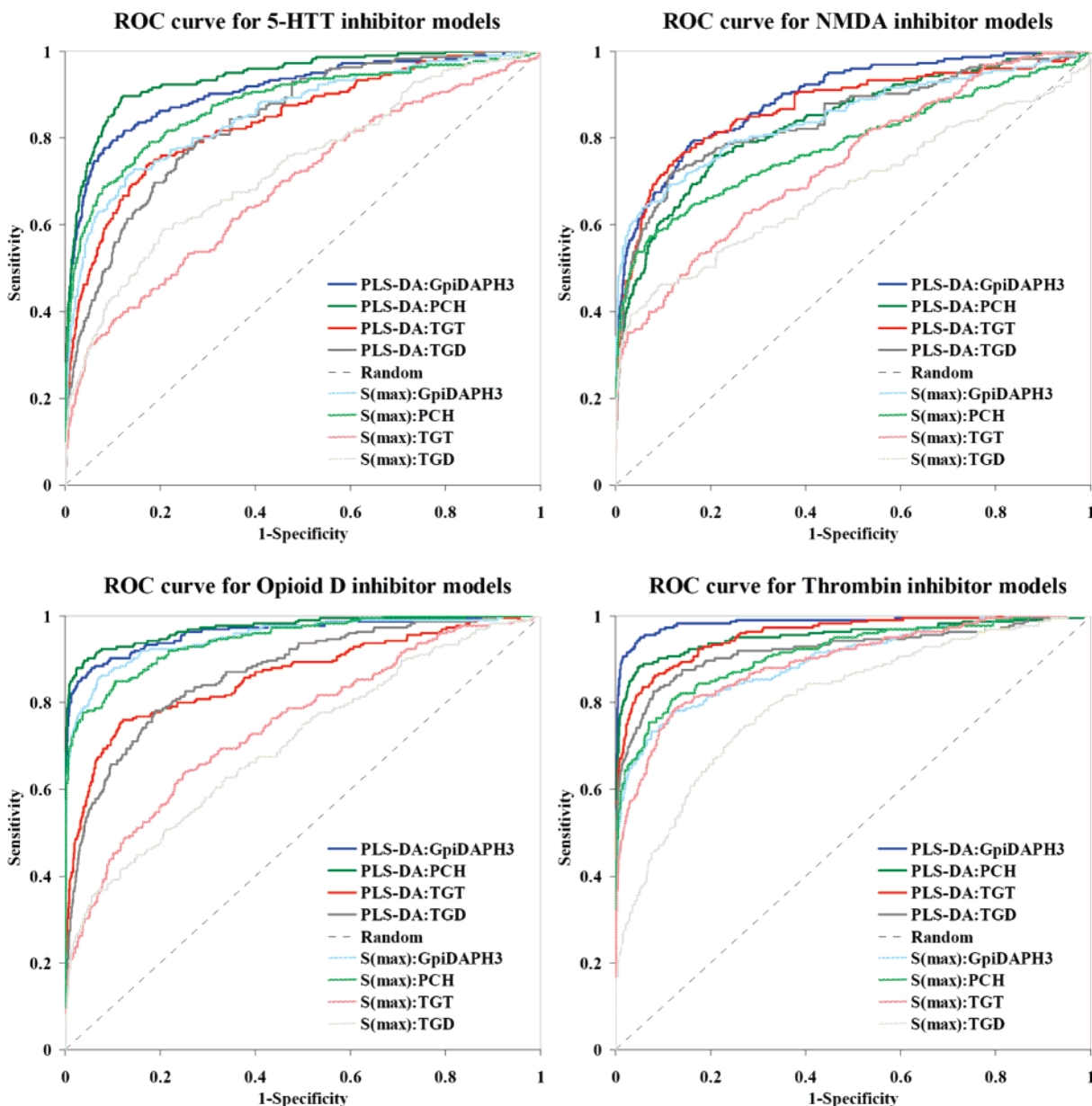


**Figure 2.** ROC plots for the test set rankings on 5-HTT, NMDA, Opioid D, and Thrombin.

however, be viewed in the context of the relatively high ROC AUC values produced by the two former fingerprint types

in general. The performance difference at the higher levels of AUC is better illustrated by studying the ROC plots for

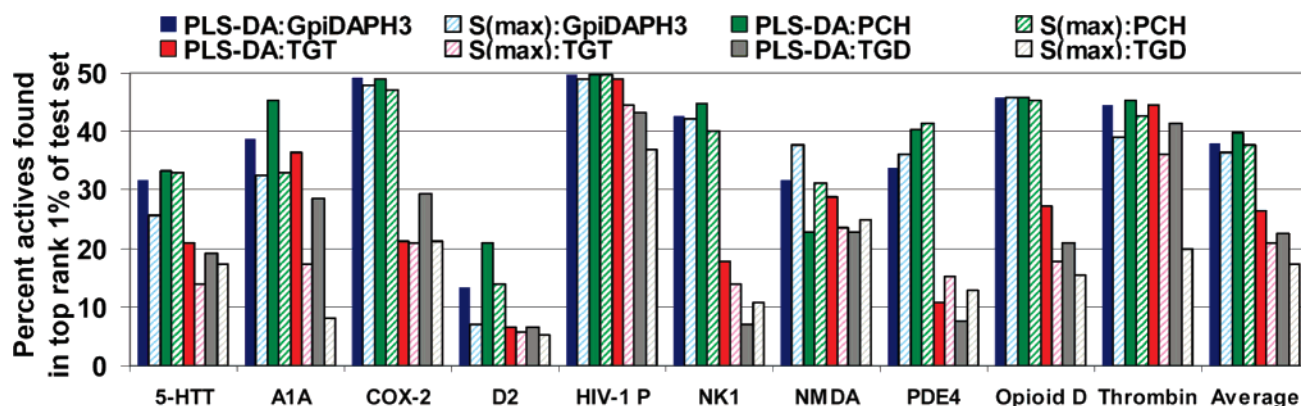


**Figure 3.** Percent actives found in the top ranking 1% of the test set using PLS-DA (solid bars) and group fusion  $S_{\max}$  (dashed bars) with the four different fingerprints; GpiDAPH3, PCH, TGT, and TGD for all 10 targets. The theoretical maximum recall at 1% of the ranked test set is 50% of the actives.

**Table 3.** Percent of Database Retrieved in Order To Recall 50% and 90% of Actives, in Class Averaged over All 10 Targets

fingerprint	PLS-DA		$S_{\max}$	
	50% recall	90% recall	50% recall	90% recall
GpiDAPH3	2.1	20.4	3.0	31.9
PCH	2.3	21.8	3.0	34.7
TGT	5.9	39.1	15.5	66.7
TGD	7.7	45.9	19.9	71.4

some of the targets. In Figure 2, the ROC plots for the 5-HTT, Opioid D, and Thrombin models show that the early discrimination for the GpiDAPH3 and PCH PLS-DA models outperforms the corresponding  $S_{\max}$  queries in terms of early recognition of actives. In particular, for the Opioid D case, where the AUC values of PLS-DA and  $S_{\max}$  are comparable, the ROC plots demonstrate the discriminative performance of the PLS-DA models much better than the AUC values.

The ROC curves for the NMDA class are less clear-cut. Here, the ROC AUC values favor the PLS-DA models, but the  $S_{\max}$  curves show the highest initial enrichments for the PCH and GpiDAPH3 fingerprints. This behavior is especially clear when we look at the initial recognition of actives in the top ranking 1% of the test set (Figure 3), where  $S_{\max}$  shows the best performance for these two fingerprints. In addition, all fingerprint types give the best initial recall using  $S_{\max}$  for the PDE4 target, but for PCH, TGT, and TGD, the overall ranking turns out best with PLS-DA. However, when we average over all 10 targets, PLS-DA gives the highest initial recognition of actives for all four fingerprints.

Upon comparison of the mean pairwise similarity of Table 1 with the ROC AUCs in Figure 1, it appears that the more diverse targets show a higher relative overall gain from using PLS-DA over  $S_{\max}$ .

Looking at the number of test set compounds that need to be sampled in order to retrieve 50% percent of the actives (Table 3), the PLS-DA method can lower this number between 23% (PCH) and 63% (TGT) percent relative to group fusion. For retrieval rates of 90% of the actives, the number of compounds sampled by PLS-DA needs only to be less than two-thirds of that sampled by  $S_{\max}$ , independent of the fingerprint type.

The overlap between the active compounds retrieved by the two different methods in the top 5% of the ranked test set is shown in Table 4. The 225 actives within each class correspond to 2% of the total test set. The overlap of the actives retrieved by PLS-DA and  $S_{\max}$  for both the Gpi-

**Table 4.** Percent of Actives Found in the Top 5% of the Database by Method and as Overlap of Methods Averaged over All 10 Targets

fingerprint	PLS-DA	$S_{\max}$	PLS-DA $\cap$ $S_{\max}$
GpiDAPH3	75.0	68.3	62.3
PCH	74.0	66.4	61.0
TGT	49.2	31.6	21.6
TGD	54.6	38.4	27.1

**Table 5.** Percent of Actives Found by PLS-DA in the Top 5% of the Database by Fingerprint Type and as Overlap/Intersection of Fingerprints Averaged over All 10 Targets

fingerprint	GpiDAPH3	PCH	TGT	TGD
GpiDAPH3	75.0	65.8	48.8	43.9
PCH		74.0	48.8	43.5
TGT			54.6	41.5
TGD				49.2

DAHP3 and PCH fingerprints is quite large, and the benefit of using both methods seems limited.

**3.3. Comparison of the Different Fingerprints.** Judging as the average overall performance for both PLS-DA and  $S_{\max}$ , the GpiDAPH3 and PCH fingerprints outperform TGT, which is again better than the TGD fingerprint. Between the fingerprint types, the average initial recognition ranks PCH slightly better than GpiDAPH3 > TGT > TGD. This pattern is, however, not consistent across all targets because the relative performance varies. The observed outcome is in agreement with the results found by Williams<sup>2</sup> in his study of the GpiDAPH3, PCH, and TGT fingerprints.

Table 5 displays the overlap between the active compounds retrieved with the different fingerprint type combinations using PLS-DA. When the actives found by selecting the top 5% are combined with both GpiDAPH3 and PCH PLS-DA models, 83% of the actives could be retrieved. Other combinations are less rewarding. In summary, the PCH fingerprint has been shown to be at least comparable to or better than the three remaining pharmacophore fingerprints. In addition, the PLS-DA procedure has, in general, shown a good performance over all targets. This high performance must mean that the model coefficients encode a general pattern that discriminates actives from inactives in 2D pharmacophore space. It is therefore interesting to take a closer look at the properties and composition of the PLS-DA models.

**3.4. Closer Look at the PLS-DA Models.** To investigate the relationship between the PLS-DA cross-validation correlation coefficient  $q^2$  and the actual model predictability,



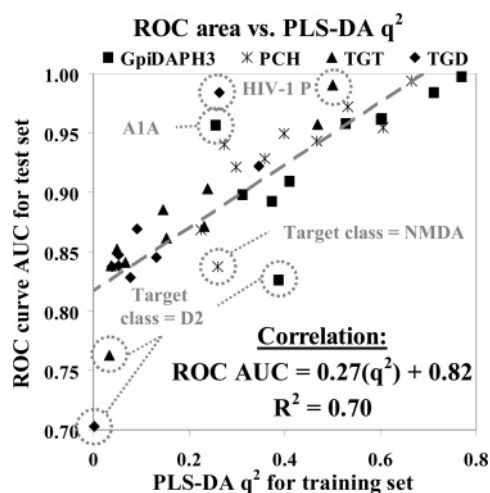


**Figure 4.** Plot of test set ROC AUC for PLS-DA models versus the cross-validation measure  $q^2$  for all four fingerprint types. The outliers that give a lower ROC AUC relative to their  $q^2$  value correspond to the D2 and NMDA target classes, which have the lowest mean pairwise Tanimoto similarity. The outliers in the top belong to the target classes A1A and HIV-1 P, which have the highest mean pairwise similarity.

we plotted the test set ROC AUC against the training set  $q^2$  for all of the PLS-DA fingerprint models (Figure 4). The outliers labeled in Figure 4 belong to either the two most diverse target classes (D2 and NMDA) or the most similar target classes (A1A and HIV-1 P) measured as the mean pairwise Tanimoto similarity. There is good agreement between the training set cross-validation  $q^2$  and the actual model performance as long as the target class is not too diverse or too similar. When the model training is based on a smaller number (25 in our case) of randomly selected actives from a very diverse class, there is a relatively higher chance that part of the test set compounds will not be well represented by the compounds in the training set. In those cases, the  $q^2$  will overestimate the models' discriminatory abilities, as we see with some of the D2 and NMDA models. The results for these outliers indicate that optimization of the  $q^2$  value might not always be the best criteria for selection of the optimal number of PCs to include in PLS-DA models that use a binary  $Y$  variable.

The number of PCs included in the model depends on the variance of the training set fingerprint bit matrix. To study the effect of including more than the first PC, which is the equivalent to the TV method, we looked at the performance of PLS-DA models using different numbers of cumulative PCs with the PCH fingerprint. Figure 5 shows ROC curves of such models for two of the better-behaved targets: Opioid D and Thrombin. The ROC plots show how the rank order of the actives in the test set markedly improves with the addition of each of the first PCs. With each PC addition, we see a small decrease in the false positive rates while the true positive rate is retained.

This behavior is desirable because improvements in the sensitivity/specificity tradeoff are of most value in the absolute top ranking part of the database, which is usually the only part relevant in large-scale virtual screening. The effect of the multiple PCs illustrated in Figure 5 is similar for the other targets except for D2 and NMDA (data not shown). The large diversity of these two target classes coupled with the random selection of actives for the training

set probably produces a fingerprint bit matrix that is not representative of the actives in the test set. This would cause  $q^2$  to be a suboptimal measure for the selection of the number of PCs to include in the model because it may introduce overfitting. This problem is well-known from the field of QSAR and concerns the selection of compounds for the training set.<sup>35</sup>

The primary effect of using multiple PCs seems to be dual because the gap in the average PLS-DA class membership score between actives and inactives increases as a consequence of higher mean scores for the actives and lower average scores for the inactives (Figure 6).

The standard deviation of the class membership score for the actives increases, while it remains close to constant for the inactive compounds. Thus, the addition of multiple PCs only seems to increase the number of true positives, while the number of false positives is kept constant or even lowered. Assuming a normal distribution around the mean of the class membership score of the inactives, a cutoff value for compound selection could be defined as the mean value plus a number of standard deviations. That is, three or four standard deviations would in theory eliminate 99.7% or 99.99% of the inactives from the selected portion.

**3.5. Model Interpretation and SAR Elucidation.** An illustrative example of the discriminatory effect of the successive PCs is the rank order of the test set compound SMDL-00132856 belonging to the Opioid D target class (Figure 7). As successive principle components are added to the PLS-DA model, the test set rank of the compound changes from 1315 to 414 to 193 to 186 to 194 as the fifth and last PC is added to the model. For comparison, the compound is ranked as number 3053 by the group fusion  $S_{\max}$  method even though there are training set compounds that seem fairly similar to the eye of a chemist. The five feature triplets projected onto the compounds in Figure 7 are weighted among the top 0.5% most important in the PLS-DA model. These five feature triplets have the 1st, 2nd, 3rd, 11th, and 21st highest coefficients scored by the compound. Together these five feature triplets correspond to 23% of the total class membership score for the compound. The projected feature triplets map well with the corresponding triplets from the training set compounds shown. On the basis of the projected feature triplets, it is possible to visualize how the individual features of the different ligands could align. A subset of the features included in the magenta, gray, and red triplets match well with the Opioid  $\delta$  primarily recognition pharmacophore reported by Loew and co-workers.<sup>36</sup> The example shown in Figure 7 represents the general picture that we see across all targets. Generally, we find that mappings of feature triplets between active compounds can help generate pharmacophore hypotheses because the feature triplets given high positive coefficients in the PLS-DA model provide information about which features that relate to activity and their mutual 2D alignment.

The reversible pharmacophore triplets identified by their high-ranking PLS-DA model coefficients can be mapped onto compounds both within the training set itself and between the training set compounds and new compounds. The mapping can help to visualize important pharmacophore patterns in 2D and provide insight into possible mutual alignments and shared modes of binding.

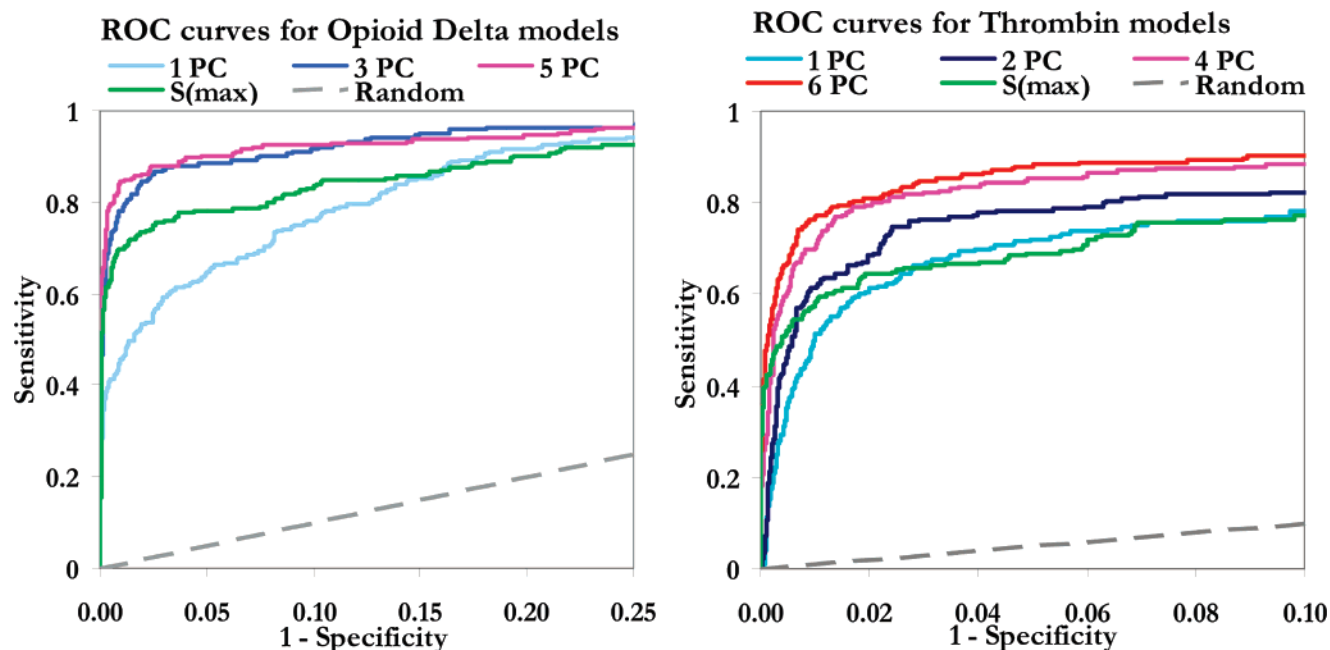


**Figure 5.** ROC plots of the PCH PLS-DA fingerprint models using different numbers of cumulative PCs (e.g., PC3 is the cumulative model of the first three PCs, etc.). Left- and right-hand side plots are for Opioid D and Thrombin, respectively. The PC1 curve corresponds to the TV. The group fusion  $S_{\max}$  curve is included for reference. Note that the scales on the horizontal and vertical axes are different.

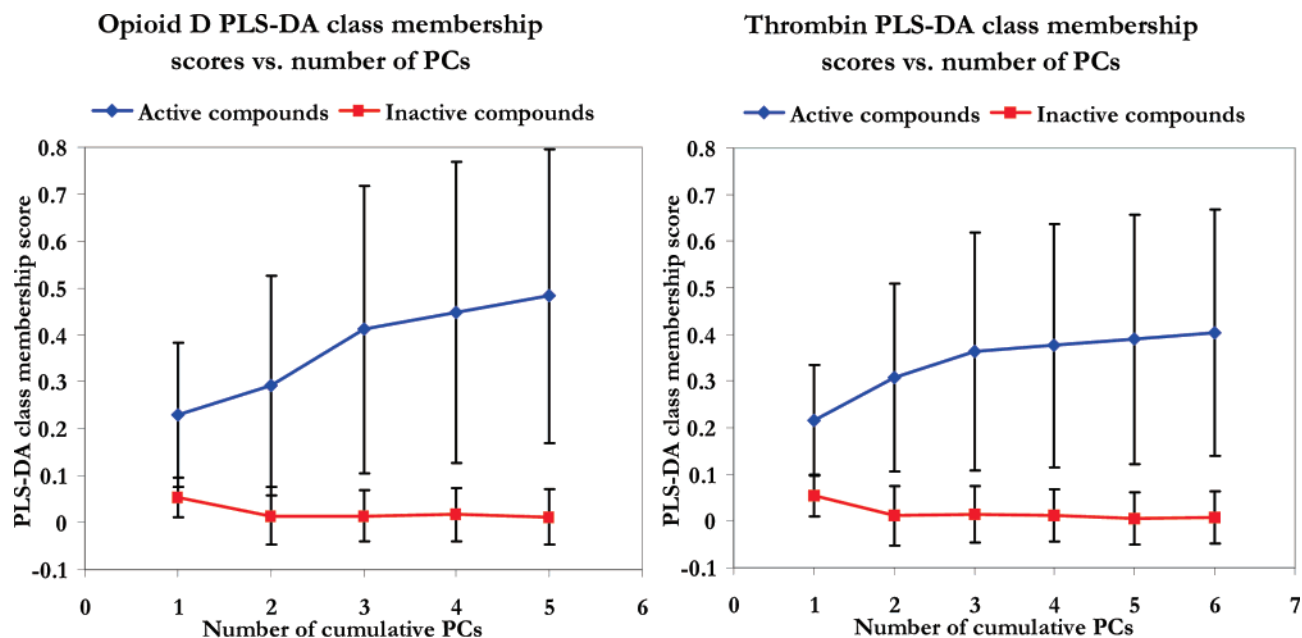


**Figure 6.** Mean-average PLS-DA class membership scores for actives (blue) and inactives (red) at different numbers of cumulative PCs. Error bars show one standard deviation from mean values. Left- and right-hand plots are for Opioid D and Thrombin PCH models, respectively.

**3.6. Mapping of 2D Feature Triplets into Three Dimensions.** To test if the 2D pharmacophore feature triplets that are identified as relating to activity by the PLS-DA models relate to the actual ligand–receptor recognition in three dimensions, we studied the four targets from our dataset that have multiple entries in the Protein Data Bank:<sup>37</sup> COX-2, HIV-1P, PDE4, and Thrombin. For each of these targets, we aligned a set of cocrystallized ligands by the X-ray structure of the protein residues surrounding the binding pocket and projected some of the top 1% highest-ranking feature triplets from the PLS-DA models using the reversible PCH fingerprint onto the aligned ligands. Because all of the

PLS-DA models were built from the same set of training compounds, they all contain the same 4122 feature triplets but have different model coefficient vectors because they were built using different active/inactive definitions. Generally, we found that high-ranking feature triplets of different ligands tend to align much better in three dimensions than low-ranking ones. Figures 8–11 show some of the results from this analysis. The feature triplets highlighted in these examples are all among the top 10 highest-ranking feature triplets shared by two or more of the cocrystallized ligands. Because the cocrystallized ligands are not all part of the training set or in any other way selected to contain all of the



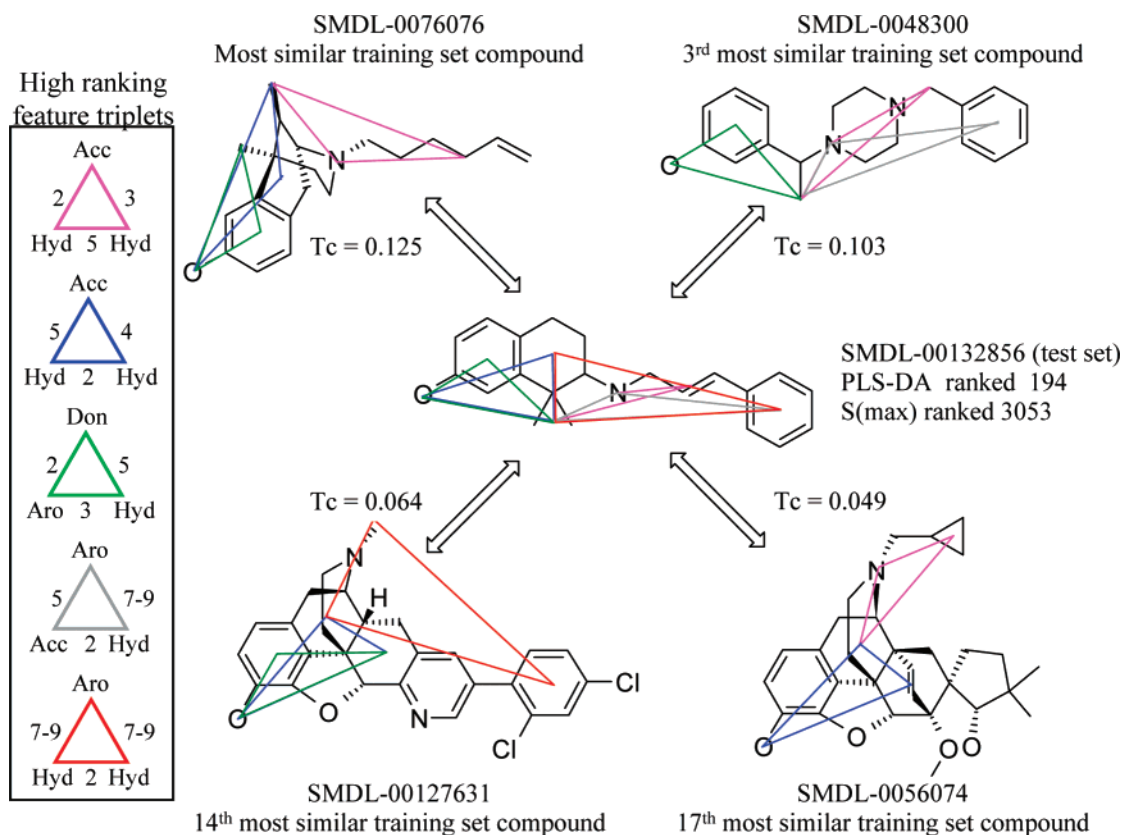


**Figure 7.** Example from the Opioid D class. The magenta, blue, green, gray, and red fingerprint feature triplets mapped onto the compounds rank as the 8th, 18th, 23rd, 71st, and 144th highest coefficients, respectively (out of 4122) for the PCH PLS-DA Opioid D model. For the feature triplets, Acc = hydrogen acceptor, Don = hydrogen donor, Aro = aromatic, and Hyd = hydrophobic, and the numbers correspond to the shortest bond counts separating the features. The Tc values indicated are the PCH Tanimoto similarities between the test set compound and selected Opioid D training set compounds.

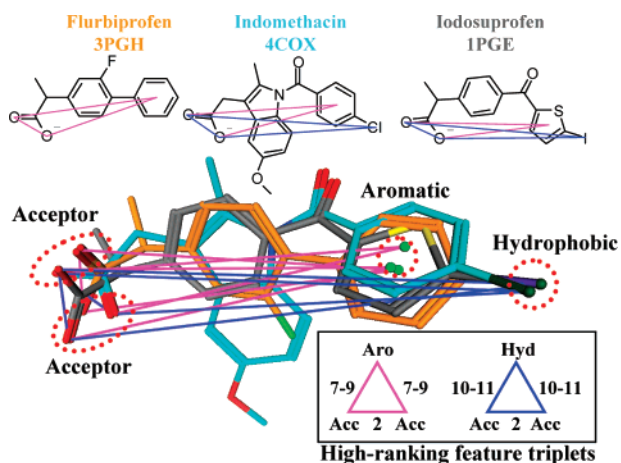


**Figure 8.** Superposition of the cocrystallized ligands of the three COX-2 PDB entries 3PGH, 4COX, and 1PGE aligned by the residues surrounding the binding pocket. The highlighted feature triplets are the highest-ranking PLS-DA model triplets shared by any of the three ligands. The magenta and blue feature triplets are ranked as the 8th and 19th highest out of 4122 feature triplets in the COX-2 PLS-DA model based on the training set. The dotted red circles indicate the individual features contributing to the highlighted feature triplets.

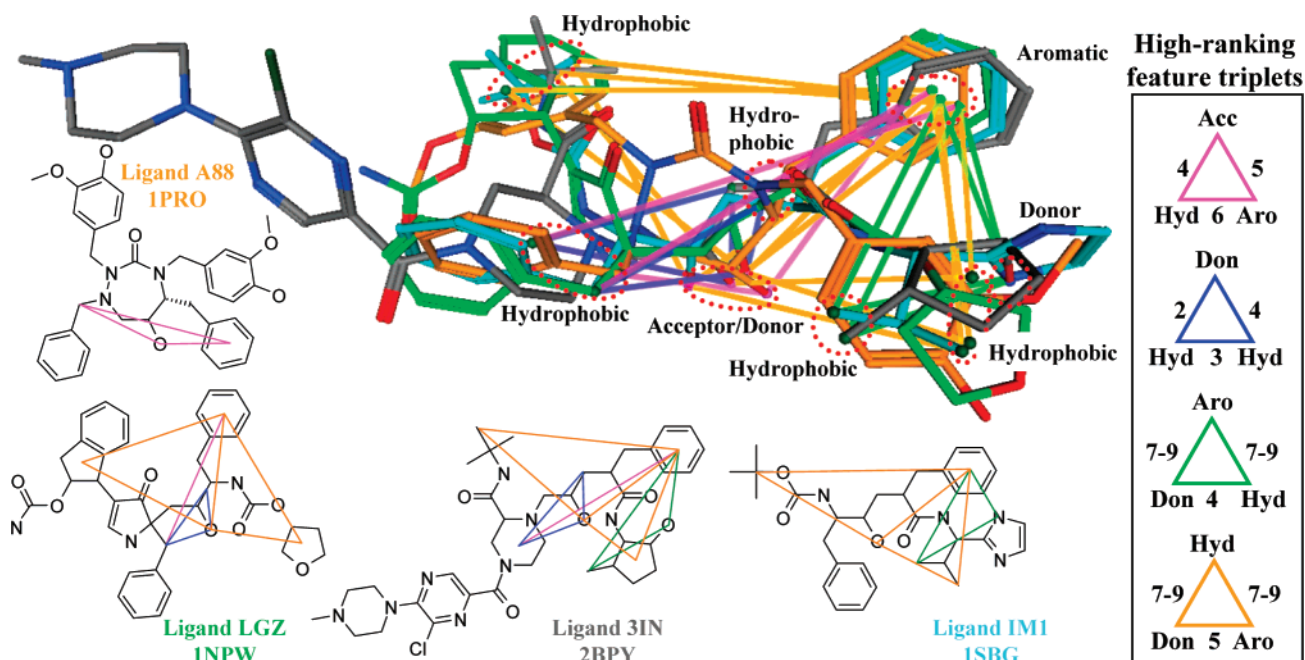
top ranking feature triplets of the models, one should not expect them to contain the first, second, third, fourth, etc., highest-ranking feature triplets of each model.

Figure 8 shows a set of aligned COX-2 inhibitors where the highlighted feature triplets overlap with very little error. The central scaffolds of the three COX-2 ligands are quite

different, but the acid acceptor groups and the aromatic and hydrophobic features on either side align nicely. The high-ranking feature triplets from the 2D PCH PLS-DA model that are projected onto the ligands correspond well with those of the COX-2 pharmacophore model proposed by Michaux et al.,<sup>38</sup> which include a hydrogen-bond acceptor and a hydrophobic group spaced by an aromatic ring in between.

Looking at Figure 9, which shows four HIV-1P inhibitors aligned by the residues of the binding site, we see a mapping of high-ranking 2D feature triplets into three dimensions. The highlighted feature triplets projected onto the ligands outline the hydroxyl groups that interact with the catalytic aspartic residues as well as a number of hydrophobic and aromatic regions of the ligands. The 3D overlay shows how the highlighted features are positioned in the areas corresponding to the hydrophobic S2, S1, S1', and S2' subpockets of the HIV-1 protease. The PCH fingerprint features identified by the model thereby match well with the typical interaction pattern found with many HIV-1P inhibitors.<sup>39</sup>

For the PDE4 example, the features projected onto the aligned ligands in Figure 10 represent the 1st, 3rd, 21st, and 23rd highest coefficients of the model. These features describe a set of conjugated hydrogen-bond acceptors flanked by a small hydrophobic group in one end linked to a bridging hydrophobic region (not present in Piclamilast), which can be attached to a hydrogen-bond acceptor. These features correspond to a subset of the pharmacophore features of the PDE4 model proposed by Fossa et al.<sup>40</sup>



**Figure 9.** Cococrystallized ligands of PDB entries 2BPY, 1PRO, 1NPW, and 1SBG aligned by the residues around the binding site. The four different feature triplets displayed show of the 9th, 13th, 23rd, and 36th highest-ranking fingerprint bits of the HIV-1P PCH PLS-DA model. Some of the feature triplets that occur multiple times in each ligand have been omitted for clarity.

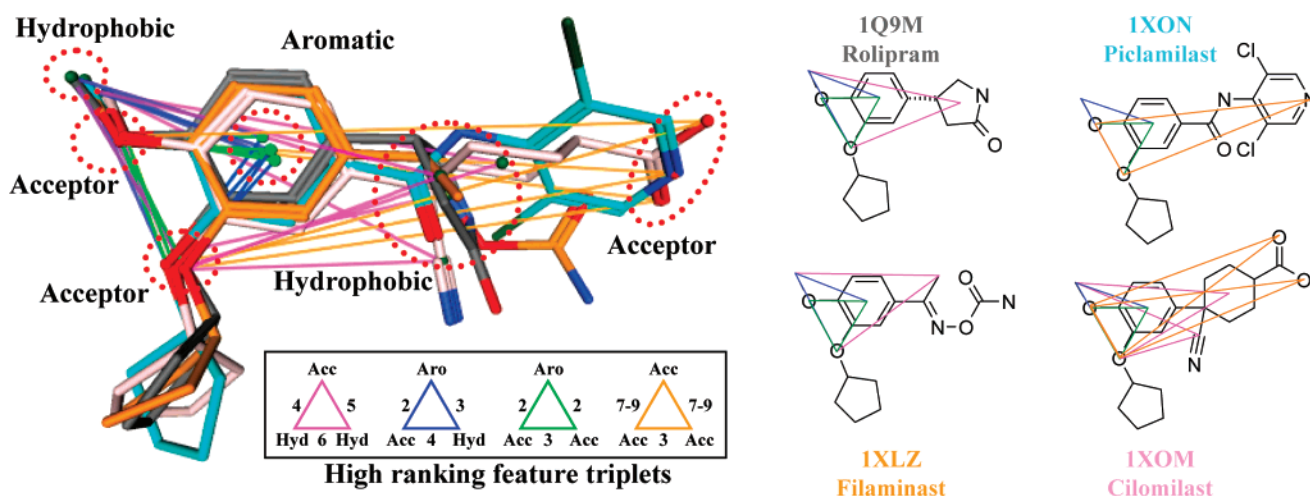


**Figure 10.** Superposition of the ligands of the PDE4 PDB entries 1Q9M, 1XON, 1XLZ, and 1XOM aligned by the residues surrounding the binding pocket. The magenta, blue, green, and orange feature triplets correspond to the PCH fingerprint features given the 1st, 3rd, 21st, and 23rd highest coefficients in the PDE4 PLS-DA model. The veratrol scaffold of all four ligands aligns and is well described by the 3rd and 21st highest-ranking features of the model. The most important feature triplet of the model is linking the two acceptors of the veratrol scaffold with a central hydrophobic region. The orange triplet describing a pure acceptor triplet shows perfect alignment for these groups of Piclamilast and Cilomilast.

The final case that we analyzed was the PCH PLS-DA model for Thrombin inhibitors. For this target, we aligned three Thrombin protein structures with cococrystallized ligands all sharing a benzamidine head group but otherwise structurally different (see Figure 11). All three ligands shared the feature triplets given the first, third, fourth, and seventh highest coefficients by the model. By projection of these feature triplets onto the aligned ligands in three dimensions, a close correspondence between 2D bond count distances and the actual 3D distances are seen. The selected 2D feature triplets identify the benzamidine head group as a dual hydrogen-bond donor and relate this group to a hydrophobic region, a hydrogen-bond acceptor, and an aromatic region. This 2D mapping corresponds to and aligns in three dimensions with the B, H1, H2, A1, and H3 features

identified by Patel et al.<sup>41</sup> as the most important features in the Thrombin pharmacophore.

The above examples illustrate how the 2D pharmacophore feature triplets identified as important for activity by the PLS-DA models relate to real 3D pharmacophore recognition between the ligand and the binding site. All of the highlighted features in Figures 8–11 correspond to actual ligand–receptor interactions that could be related to pharmacophore models reported in the literature or otherwise known binding modes confirmed by X-ray structures. Thus, the enrichment produced by these models in virtual screening should not be just an artifact of high similarity between training set and test set ligands. It appears that the PLS-DA model captures a sum of some of the ligand pharmacophore features that is recognized by the target and that this sum is a very powerful

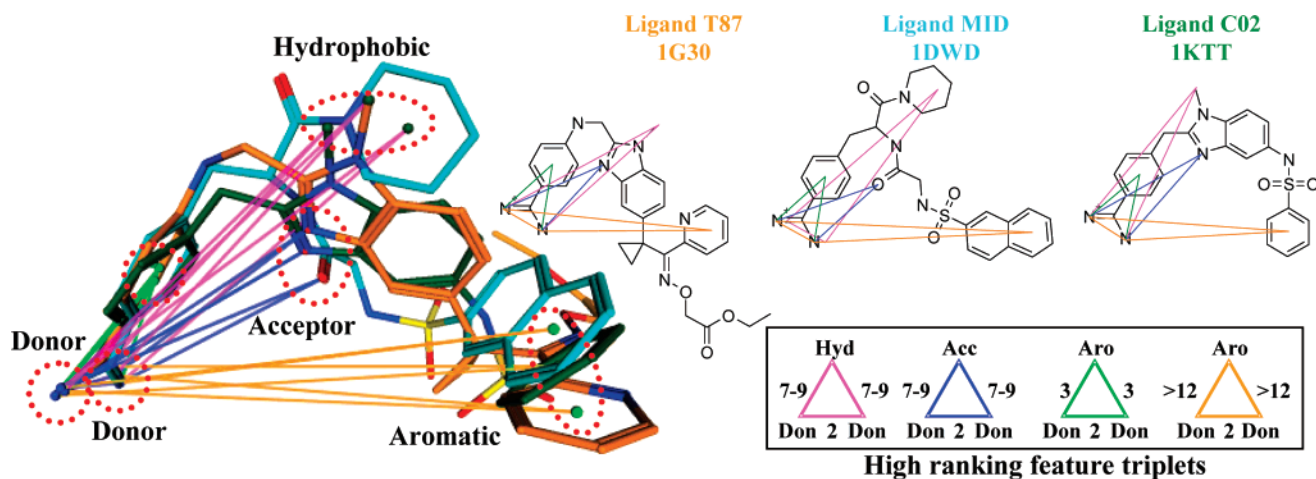


**Figure 11.** Three Thrombin inhibitors aligned by the residues surrounding the binding site in the PDB entries 1G30, 1DWD, and 1KTT. All three ligands share the benzamidine head group but are otherwise diverse. The magenta, blue, green, and orange PCH feature triplets are ranked first, third, fourth, and seventh by the Thrombin PLS-DA model. Besides the pharmacophore features of the benzamidine group, the model identity includes a common hydrophobic region, a hydrogen-acceptor position, and an overlap of aromatic rings. Note how the labeled hydrogen-acceptor groups (blue triplet) overlap in terms of both position and directionality.

discriminative factor as well as a source of direct SAR information. The use of 2D pharmacophore fingerprints relative to their 3D counterparts eliminates the issue of dealing with multiple conformations of both training and test set compounds. Computationally this is an advantage, but it also represents a potential loss of information, because the 3D fingerprints are able to give a richer description of flexible molecules, some of which might bind in a collapse conformation.<sup>42</sup> Such collapsed binding modes are, however, not as common as one might think because it has been shown that flexible ligands have a general tendency to bind in extended conformations.<sup>43</sup> The four-point 3D pharmacophore fingerprints are, however, able to encode unique properties like the volume and chirality of the compounds<sup>44</sup> that cannot be approximated by the current 2D pharmacophore fingerprints. The PLS-DA method for virtual screening and SAR elucidation could just as well be used with, e.g., modal or union 3D three- or four-point fingerprints as with 2D fingerprints. Because of the increased computational demands of extending the analysis to 3D fingerprints and the popularity and efficiency<sup>45</sup> of the 2D fingerprints, we chose to limit our current study to the latter.

We have found the combination of the PLS-DA method and reversible 2D pharmacophore feature triplets to be a useful tool for both virtual screening and SAR elucidation. The models derived from a relatively low number of actives seem to capture information that relates to the general ligand–receptor recognition process. This information can be interpreted in terms of the identification of important pharmacophore features and their relative alignment among a set of active ligands.

Given a reasonable 2D alignment of pharmacophore features between a set of ligands, it should be possible to generate a reasonable 3D alignment of the ligands via molecular force fields and a set of interligand feature–feature constraints. This alignment can then form the basis for a 3D pharmacophore model describing essential features of the ligand–receptor recognition.

We therefore propose to use the information derived by the PLS-DA models to create interligand 2D pharmacophore feature alignment pairs for use in manual and automated 3D

ligand alignment procedures. If the set of possible feature pair constraints were derived from a pharmacophore fingerprint PLS-DA model trained on a set of actives and inactives, it would greatly limit the vast combinatorial space comprised of all possible feature pair combinations that exist between a set of flexible ligands. This information could, for example, be used to populate the feature–feature alignment chromosome of a GASP<sup>13</sup>-like alignment procedure. This improvement would initiate the superposition of flexible ligands in the relevant subspace of the feature–feature combinatorial space in contrast to random positions.

In addition, we believe that the introduction of a fuzzy graph distance binning scheme, like the one recently introduced by Horvath and co-workers,<sup>46</sup> in combination with the PLS-DA method would improve the value of both the virtual screening and the SAR elucidation process just described. Small variations in intermediate bond distance counts can easily span the same distances through space, and overlapping graph distance binning would therefore allow for matching of feature triplets with small variation in the separating graph distances. This introduction of fuzziness could also account for some part of the flexibility of the binding site to accommodate ligands of varying size.<sup>47</sup> The fuzziness could therefore soften some of the conceptual differences between the 2D and 3D descriptor worlds.

#### 4. CONCLUSION

The result of the retrospective virtual screening experiment showed that on average the PLS-DA models were better than the group fusion  $S_{\max}$  similarity searching method, in terms of both ROC AUC and early recognition. Upon comparison of the different fingerprint types, their relative performance was, in general, independent of the ranking method. GpiDAPH3 and PCH clearly outperformed TGT, which again was better than the simpler TGD fingerprint. Measured as early recognition in the top 1% of the ranked test set, PCH marginally outperformed GpiDAPH3, and again these two showed better performance than the TGT and TGD fingerprints. However, the results did vary across the 10 targets, but, in general, the longer and more complex pharmacophore



fingerprints GpiDAPH3 and PCH were superior to the simpler TGT and TGD fingerprints for both PLS-DA and  $S_{\max}$ . The overlap of the compounds retrieved by PLS-DA and  $S_{\max}$  methods was quite large (Table 4). The overlap observed was larger when the active compounds retrieved using only PLS-DA were compared with two different fingerprints (Table 5). These results indicated that it would be more beneficial to use two different fingerprint types than to use both methods with the same fingerprint if two virtual screens were to be performed on the same target.

The PLS cross-validation statistics  $q^2$  seems to be a good indicator for the discriminative power of PLS-DA pharmacophore fingerprint models even with the relatively small training set sizes used in this study, at least as long as the actives in the training set are not too remotely related to the actives in the test set. In general, the use of multiple PCs gives higher initial enrichment. This behavior suggests that PLS-DA should be preferred over the TV method for virtual screening applications.

Our analysis of the combination of PLS-DA with the reversible 2D PCH fingerprint showed that this mixture is a useful tool for SAR elucidation. The model interpretation provided information on the pharmacophore features important for the ligand–target recognition process. In addition, the method can be used to guide the alignment of ligands and for visualization of common pharmacophore feature combinations across sets of ligands. The experiment of mapping 2D feature triplets, identified by the PLS-DA model to be important for activity, onto aligned crystal structures of a set of ligands showed a clear alignment of the 2D feature triplets in Cartesian space. The good performance of 2D pharmacophore fingerprints for virtual screening can therefore be explained at the structural level because the 2D fingerprints relate directly to the 3D pharmacophore recognition between the ligand and the binding site.

#### ACKNOWLEDGMENT

The authors thank Chris Williams for stimulating discussions and for making the reversible fingerprints and the visualization tools available via the SVL exchange.<sup>48</sup> We thank Tommy Liljefors and Jonathan S. Mason for careful reading of the manuscript and valuable suggestions. In addition, S.A. thanks H. Lundbeck A/S and the Danish Ministry of Science, Technology and Innovation for funding a Ph.D. scholarship.

**Supporting Information Available:** Lists of training and test set compounds with target class information. For compounds coming from Wombat, only database ids can be given. For the decoy set, the structures are included in SMILES format. This material is available free of charge via the Internet at <http://pubs.acs.org>.

#### REFERENCES AND NOTES

- Hert, J.; Willett, P.; Wilton, D. J. Comparison of fingerprint-based methods for virtual screening using multiple bioactive reference structures. *J. Chem. Inf. Comput. Sci.* **2004**, *44* (3), 1177–1185.
- Williams, C. Reverse fingerprinting, similarity searching by group fusion and fingerprint bit importance. *Mol. Diversity* **2006**, *10* (3), 311–332.
- Weaver, D. C. Applying data mining techniques to library design, lead generation and lead optimization. *Curr. Opin. Chem. Biol.* **2004**, *8* (3), 264–270.
- PubChem, National Center for Biotechnology Information. <http://pubchem.ncbi.nlm.nih.gov/> (accessed Sept 2007).
- Wombat World of Molecular BioActivity, version 2005.02; Sunset Molecular Discovery: Santa Fe, NM, 2005.
- Lengauer, T.; Lemmen, C.; Rarey, M.; Zimmermann, M. Novel technologies for virtual screening. *Drug Discovery Today* **2004**, *9* (1), 27–34.
- Keseru, G. M.; Makara, G. M. Hit discovery and hit-to-lead approaches. *Drug Discovery Today* **2006**, *11* (15–16), 741–748.
- Eckert, H.; Bajorath, J. Molecular similarity analysis in virtual screening: foundations, limitations and novel approaches. *Drug Discovery Today* **2007**, *12* (5–6), 225–233.
- Whittle, M.; Gillet, V. J.; Willett, P.; Alex, A.; Loesel, J. Enhancing the effectiveness of virtual screening by fusing nearest neighbor lists: A comparison of similarity coefficients. *J. Chem. Inf. Comput. Sci.* **2004**, *44* (5), 1840–1848.
- Stahura, F. L.; Bajorath, M. New methodologies for ligand-based virtual screening. *Curr. Pharm. Des.* **2005**, *11* (9), 1189–1202.
- Plewczynski, D.; Spieser, S. A. H.; Koch, U. Assessing different classification methods for virtual screening. *J. Chem. Inf. Model.* **2006**, *46* (3), 1098–1106.
- Villar, H. O.; Hansen, M. R.; Kho, R. Substructural analysis in drug discovery. *Curr. Comput.-Aided Drug Des.* **2007**, *3* (1), 59–67.
- Jones, G.; Willett, P.; Glen, R. C. A genetic algorithm for flexible molecular overlay and pharmacophore elucidation. *J. Comput.-Aided Mol. Des.* **1995**, *9* (6), 532–549.
- Greene, J.; Kahn, S.; Savoj, H.; Sprague, P.; Teig, S. Chemical Function Queries for 3D Database Search. *J. Chem. Inf. Comput. Sci.* **1994**, *34* (6), 1297–1308.
- Molecular Operating Environment (MOE), version 2006.08; Chemical Computing Group: Montreal, Quebec, Canada, 2006.
- Renner, S.; Schneider, G. Fuzzy pharmacophore models from molecular alignments for correlation-vector-based virtual screening. *J. Med. Chem.* **2004**, *47* (19), 4653–4664.
- Sorich, M. J.; Miners, J. O.; McKinnon, R. A.; Winkler, D. A.; Burden, F. R.; Smith, P. A. Comparison of linear and nonlinear classification algorithms for the prediction of drug and chemical metabolism by human UDP-glucuronosyltransferase isoforms. *J. Chem. Inf. Comput. Sci.* **2003**, *43* (6), 2019–2024.
- Sheridan, R. P.; Nachbar, R. B.; Bush, B. L. Extending the trend vector—the trend matrix and sample-based partial least-squares. *J. Comput.-Aided Mol. Des.* **1994**, *8* (3), 323–340.
- Pirard, B.; Pickett, S. D. Classification of kinase inhibitors using BCUT descriptors. *J. Chem. Inf. Comput. Sci.* **2000**, *40* (6), 1431–1440.
- Evers, A.; Hessler, G.; Matter, H.; Klabunde, T. Virtual screening of biogenic amine-binding G-protein coupled receptors: Comparative evaluation of protein- and ligand-based virtual screening protocols. *J. Med. Chem.* **2005**, *48* (17), 5448–5465.
- Carhart, R. E.; Smith, D. H.; Venkataraghavan, R. Atom pairs as molecular features in structure activity studies—Definition and applications. *J. Chem. Inf. Comput. Sci.* **1985**, *25* (2), 64–73.
- Cramer, R. D.; Redl, G.; Berkoff, C. E. Substructural analysis. Novel approach to the problem of drug design. *J. Med. Chem.* **1974**, *17* (5), 533–535.
- Wilton, D.; Willett, P.; Lawson, K.; Mullier, G. Comparison of ranking methods for virtual screening in lead-discovery programs. *J. Chem. Inf. Comput. Sci.* **2003**, *43* (2), 469–474.
- SIMCA-P+, version 11; Umetrics AB: Umeå, Sweden, 2006.
- Wold, S.; Sjostrom, M.; Eriksson, L. PLS-regression: a basic tool of chemometrics. *Chemom. Intell. Lab. Syst.* **2001**, *58* (2), 109–130.
- Olah, M.; Bologa, C.; Oprea, T. I. An automated PLS search for biologically relevant QSAR descriptors. *J. Comput.-Aided Mol. Des.* **2004**, *18* (7–9), 437–449.
- 3D QSAR in Drug Design; Kubinyi, H., Ed.; ESCOM Science Publishers BV: Leiden, The Netherlands, 1993.
- Xia, X. Y.; Maliski, E. G.; Gallant, P.; Rogers, D. Classification of kinase inhibitors using a Bayesian model. *J. Med. Chem.* **2004**, *47* (18), 4463–4470.
- Franke, L.; Byvatov, E.; Werz, O.; Steinhilber, D.; Schneider, P.; Schneider, G. Extraction and visualization of potential pharmacophore points using support vector machines: Application to ligand-based virtual screening for COX-2 inhibitors. *J. Med. Chem.* **2005**, *48* (22), 6997–7004.
- Chen, B. N.; Harrison, R. F.; Papadatos, G.; Willett, P.; Wood, D. J.; Lewell, X. Q.; Greenidge, P. A.; Stiefl, N. Evaluation of machine-learning methods for ligand-based virtual screening. *J. Comput.-Aided Mol. Des.* **2007**, *21*, 53–62.
- Willett, P. Similarity-based virtual screening using 2D fingerprints. *Drug Discovery Today* **2006**, *11* (23–24), 1046–1053.
- Triballeau, N.; Acher, F.; Brabet, I.; Pin, J. P.; Bertrand, H. O. Virtual screening workflow development guided by the “receiver operating characteristic” curve approach. Application to high-throughput docking

- on metabotropic glutamate receptor subtype 4. *J. Med. Chem.* **2005**, 48 (7), 2534–2547.
- (33) Witten, I.; Frank, E. *Data Mining, Practical Machine Learning Tools and Techniques*; Morgan Kaufmann Publishers–Elsevier: Burlington, MA, 2005.
- (34) Truchon, J. F.; Bayly, C. I. Evaluating virtual screening methods: Good and bad metrics for the “early recognition” problem. *J. Chem. Inf. Model.* **2007**, 47 (2), 488–508.
- (35) Golbraikh, A.; Shen, M.; Xiao, Z. Y.; Xiao, Y. D.; Lee, K. H.; Tropsha, A. Rational selection of training and test sets for the development of validated QSAR models. *J. Comput.-Aided Mol. Des.* **2003**, 17 (2), 241–253.
- (36) Huang, P.; Kim, S.; Loew, G. Development of a common 3D pharmacophore for delta-opioid recognition from peptides and non-peptides using a novel computer program. *J. Comput.-Aided Mol. Des.* **1997**, 11 (1), 21–28.
- (37) Protein Data Bank, RCSB. <http://www.pdb.org> (accessed Sept 2007).
- (38) Michaux, C.; de Leval, X.; Julemont, F.; Dogne, J. M.; Pirotte, B.; Durant, F. Structure-based pharmacophore of COX-2 selective inhibitors and identification of original lead compounds from 3D database searching method. *Eur. J. Med. Chem.* **2006**, 41 (12), 1446–1455.
- (39) Han, Q.; Chang, C. H.; Li, R. H.; Ru, Y.; Jadhav, P. K.; Lam, P. Y. S. Cyclic HIV protease inhibitors: Design and synthesis of orally bioavailable, pyrazole P2/P2' cyclic ureas with improved potency. *J. Med. Chem.* **1998**, 41 (12), 2019–2028.
- (40) Fossa, P.; Menozzi, G.; Mosti, L. An updated topographical model for phosphodiesterase 4 (PDE4) catalytic site. *Quant. Struct.–Act. Relat.* **2001**, 20 (1), 17–22.
- (41) Patel, Y.; Gillet, V. J.; Bravi, G.; Leach, A. R. A comparison of the pharmacophore identification programs: Catalyst, DISCO and GASP. *J. Comput.-Aided Mol. Des.* **2002**, 16 (8–9), 653–681.
- (42) Mason, J. S.; Good, A. C.; Martin, E. J. 3-D Pharmacophores in drug discovery. *Curr. Pharm. Des.* **2001**, 7 (7), 567–597.
- (43) Perola, E.; Charifson, P. S. Conformational Analysis of Drug-Like Molecules Bound to Proteins: An Extensive Study of Ligand Reorganization upon Binding. *J. Med. Chem.* **2004**, 2004 (47), 2499–2510.
- (44) Mason, J. S.; Morize, I.; Menard, P. R.; Cheney, D. L.; Hulme, C.; Labaudiniere, R. F. New 4-point pharmacophore method for molecular similarity and diversity applications: Overview of the method and applications, including a novel approach to the design of combinatorial libraries containing privileged substructures. *J. Med. Chem.* **1999**, 42 (17), 3251–3264.
- (45) Sheridan, R. P.; Kearsley, S. K. Why do we need so many chemical similarity search methods? *Drug Discovery Today* **2002**, 7 (17), 903–911.
- (46) Bonachera, F.; Parent, B.; Barbosa, F.; Froloff, N.; Horvath, D. Fuzzy tricentric pharmacophore fingerprints. 1. Topological fuzzy pharmacophore triplets and adapted molecular similarity scoring schemes. *J. Chem. Inf. Model.* **2006**, 46 (6), 2457–2477.
- (47) Davis, A. M.; Teague, S. J. Hydrogen Bonding, Hydrophobic Interactions, and Failure of the Rigid Receptor Hypothesis. *Angew. Chem., Int. Ed.* **1999**, 38, 736–749.
- (48) Chemical Computing Group. SVL Exchange. <http://svl.chemcomp.com> (accessed May 2007).

CI700356W